



Comparison of Fracture Behavior Between Nanocomposites Reinforced with Straight and Sinusoidal Carbon Nanotubes

Mahdiye Hamedi *

Shahrebabak Azad University, Kerman, Iran

ABSTRACT: This research focuses on the impact of Carbon Nanotube geometry and dispersion on fracture behavior within nanocomposite materials. Specifically, straight and sinusoidal configurations were investigated under both ordered and disordered spatial arrangements. The analysis employed finite element methods and micromechanical techniques to explore crack propagation paths and evaluate interactions at the Carbon Nanotube-matrix interface. Fracture toughness across the four configurations was assessed based on the Maximum Tangential Stress criterion and the maximum energy release rate. The study concludes with a comparative evaluation of the findings and previously published results, confirming the reliability of the proposed modeling approach.

Review History:

Received: Nov. 12, 2024

Revised: Mar. 06, 2025

Accepted: Mar. 15, 2025

Available Online: Mar. 29, 2025

Keywords:

Nanocomposite

Contact Surface

Crack Growth

Finite Element

Micromechanical

1- Introduction

Gojny et al. examined the influence of incorporating carbon nanotubes (CNTs) on the mechanical strength of polymer composites, emphasizing that nanotubes with a high aspect ratio and micron-scale lengths substantially enhance performance, particularly when uniformly dispersed [1]. Quaresimin and colleagues, through a multi-scale modeling approach, explored the toughening effects of spherical nanoparticles in polymers, validating their models by cross-referencing with established literature [2].

Meliani et al. conducted fracture testing on epoxy matrices filled with nanoclay using notched three-point bending techniques. Their results demonstrated that when the notch radius was below 1 mm, the toughness remained stable [3]. Similarly, Shadlou et al. evaluated various carbon nanoparticle shapes and concluded that spherical forms delivered superior mode II fracture resistance in epoxy nanocomposites [4].

Golestanian and Hamedi investigated the significance of CNT morphology and layout in nanocomposite failure, showing that stress concentrations at the nanotube tips frequently serve as initiation sites for damage [5]. Hosseini et al. addressed stability challenges in CNT-reinforced plates sandwiched between piezoelectric layers under supersonic flow, noting improvements in both dynamic stability and pressure tolerance [6].

Dastjerdi and colleagues studied the vibrational behavior of rotating conical structures enhanced with CNTs and proposed a novel analytical method for handling perforated geometries [7]. Givi et al. analyzed the flutter and vibration behavior of sandwich cylindrical shells using reinforced honeycomb cores, concluding that additional CNT stiffening did not always yield better aeroelastic performance [8].

Khodami Maraghi focused on structural deformation and load transfer within composite sandwich plates, offering insights applicable to aerospace and defense systems [9]. Akbas et al. observed that CNT distribution and pattern significantly influenced deflection behavior in composite beams under dynamic loading, with X Beams showing greater stiffness [10]. Hamedi et al. evaluated fracture energy using a hybrid approach that combined finite element simulations with FESEM imaging, offering an accurate depiction of CNT-enhanced nanocomposites [11].

From this literature review, it is evident that CNTs are rarely perfectly straight in real-world applications, often displaying curvature or waviness. Despite extensive work, few studies have addressed fracture in sinusoidal CNT-reinforced composites, and the role of CNT distribution on fracture toughness remains underexplored.

This study aims to fill that gap by systematically analyzing the effects of CNT geometry (straight vs. sinusoidal) and distribution (uniform vs. random) on crack propagation and toughness. Unlike prior work that assumes ideal interfacial

*Corresponding author's email: mahdiyehamedi@yahoo.com



bonding, this research emphasizes the influence of the CNT–matrix contact surface. Simulations include polymer matrices reinforced with both types of CNTs, applying finite element modeling and micromechanical analysis to evaluate failure behavior.

Initially, straight CNTs with uniform alignment are examined, and their KI–KII fracture response is computed. These outcomes are then compared to published results for model validation. Subsequently, models incorporating sinusoidal CNTs in both uniform and random arrangements are studied. Fracture toughness is assessed using Maximum Tangential Stress (MTS) and energy release rate (G) criteria. Comparative analysis underscores the pivotal influence of CNT geometry and spatial layout on failure mechanisms in nanocomposites.

2- Analysis

To investigate the effects of CNT geometry and spatial arrangement on crack propagation, a combination of finite element analysis (FEA) and micromechanical modeling was used. The representative volume element (RVE), based on the configuration introduced by Chen and Liu [12], was employed as the simulation domain. Both straight and sinusoidal CNTs were modeled with either random or uniform distributions within the matrix. Across all simulated configurations, a perfect bonding condition was assumed between the CNTs and the matrix. Consistent CNT weight fractions—1%, 1.5%, and 3%—were applied to ensure a fair comparison among the different designs. Details of the modeling process and structural response for each CNT configuration are presented in the following subsections. In the case of straight CNTs with uniform alignment, the applied boundary conditions included a combination of axial tensile and tangential loading. Crack paths and fracture behavior were analyzed using ABAQUS software, which revealed mode-specific toughness trends depending on CNT orientation and placement. Randomly distributed straight CNTs were also investigated under similar loading conditions. Fracture toughness was extracted for each case, providing insights into the role of randomness in reinforcing efficiency.

For consistency and comparative analysis, CNT weight fractions of 1%, 1.5%, and 3% were applied across all four nanocomposite configurations. The following sections provide a detailed discussion of the modeling and analysis procedures for each type of nanocomposite.

2- 1- Analysis of RVE Reinforced with Straight CNTs

To investigate the effects of CNT geometry and spatial arrangement on crack propagation, a combination of finite element analysis (FEA) and micromechanical modeling was used. The representative volume element (RVE), based on the configuration introduced by Chen and Liu [12], was employed as the simulation domain. Both straight and sinusoidal CNTs were modeled with either random or uniform distributions within the matrix. Across all simulated configurations, a perfect bonding condition was assumed between the CNTs and the matrix. Consistent CNT weight fractions—1%, 1.5%,

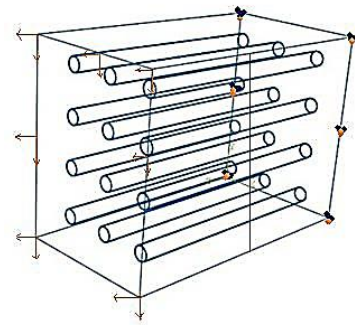


Fig. 1. The FEA model of the RVE under mixed mode loading (uniformly-distributed).

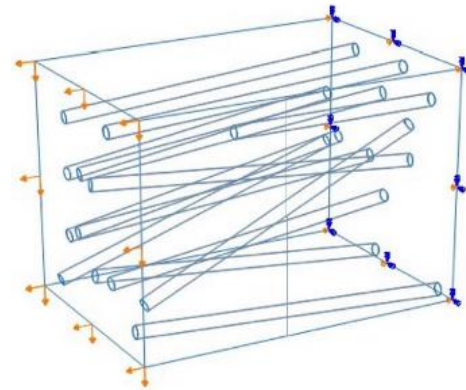


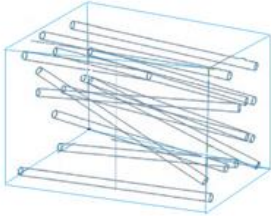
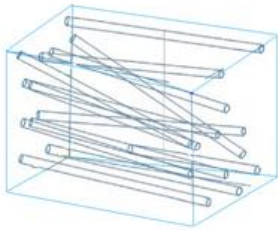
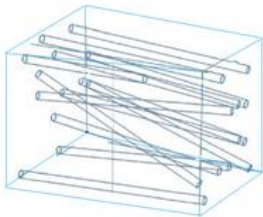
Fig. 2. The FEA model of the RVE under mixed mode loading (randomly distributed).

and 3%—were applied to ensure a fair comparison among the different designs. Details of the modeling process and structural response for each CNT configuration are presented in the following subsections. In the case of straight CNTs with uniform alignment, the applied boundary conditions included a combination of axial tensile and tangential loading. Crack paths and fracture behavior were analyzed using ABAQUS software, which revealed mode-specific toughness trends depending on CNT orientation and placement. Randomly distributed straight CNTs were also investigated under similar loading conditions. Fracture toughness was extracted for each case, providing insights into the role of randomness in reinforcing efficiency.

In the second set of models, straight carbon nanotubes were embedded within the matrix in a randomly distributed manner, as illustrated in Figure 2. To represent the random distribution, three different cases of nanotube arrangements were examined. The fracture toughness values for both Mode I and Mode II were determined and are presented in Table 1.

The results of this comparison, showed that the maximum difference percent is 8.

Table 1. Comparison of fracture toughnesses of three cases of straight nanotubes distribution.

Distribution of carbon nanotubes	K_I (MPa. m ^{0.5})	K_{II} (MPa. m ^{0.5})	Difference percent (%)
	2	1.5	$K_I=7.5$
	1.85	1.38	$K_{II}=8$
	1.93	1.45	$K_I=3.5$ $K_{II}=3.33$

2- 2- Analysis of the RVE Reinforced with Sinusoidal CNTs

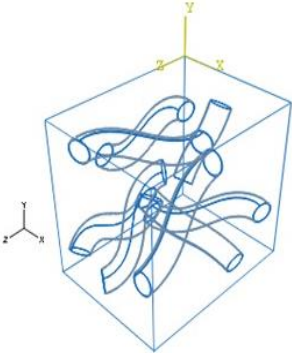
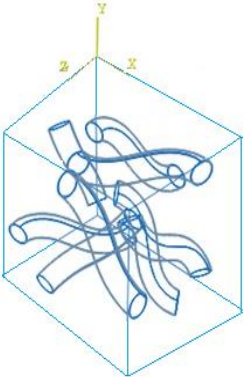
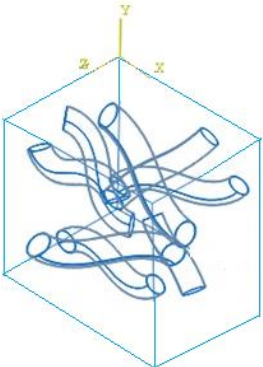
To investigate the effects of CNT geometry and spatial arrangement on crack propagation, a combination of finite element analysis (FEA) and micromechanical modeling was used. The representative volume element (RVE), based on the configuration introduced by Chen and Liu [12], was employed as the simulation domain. Both straight and sinusoidal CNTs were modeled with either random or uniform distributions within the matrix. Across all simulated configurations, a perfect bonding condition was assumed between the CNTs and the matrix. Consistent CNT weight fractions—1%, 1.5%, and 3%—were applied to ensure a fair comparison among the different designs. Details of the modeling process and structural response for each CNT configuration are presented in the following subsections. In the case of straight CNTs with uniform alignment, the applied boundary conditions included a combination of axial tensile and tangential loading. Crack paths and fracture behavior were analyzed using ABAQUS software,

which revealed mode-specific toughness trends depending on CNT orientation and placement. Randomly distributed straight CNTs were also investigated under similar loading conditions. Fracture toughness was extracted for each case, providing insights into the role of randomness in reinforcing efficiency.

Additionally, another model was developed in which sinusoidal CNTs were randomly distributed in the matrix, as shown in Figure 3(b). In this case, the RVE dimensions were set to 60 × 70 × 79 nm in the x, y, and z directions. Eight CNTs, each 50 nm in length with an outer diameter of 10 nm, were incorporated into this RVE. The curvature radius of the CNTs remained 22 nm, maintaining a CNT weight fraction of 1.5%. To represent randomness in distribution, three different cases of sinusoidal nanotube arrangements were examined. The fracture toughness values for both Mode I and Mode II were determined and are presented in Table 2.

The results of this comparison showed that the maximum difference percent is 7.24.

Table 2. comparison fracture toughnesses of three cases of sinusoidal nanotubes distribution.

Distribution of carbon nanotubes	K_I (MPa. m ^{0.5})	K_{II} (MPa. m ^{0.5})	Difference percent (%)
	2.22	1.75	$K_I= 7.24$
	2.05	1.65	$K_{II}= 5.7$
	2.1	1.71	$K_I= 5$ $K_{II}= 2.29$

2- 3- Fracture Criteria for Mixed-Mode Loading

Various failure criteria have been introduced to characterize mixed-mode fracture behavior in different engineering materials. In this study, numerical data were analyzed using two widely recognized fracture criteria: the Maximum Tangential Stress (MTS) Criterion and the Maximum Energy Release Rate (G) Criterion. A brief overview of these criteria is provided in the following section.

2- 4- Maximum Tangential Stress (MTS) Criterion

For a crack subjected to combined Mode I and Mode II loading, the tangential stress near the crack tip can be expressed in a polar coordinate system using the singular term formulation (Ayatollahi et al., 2011):

$$\sigma_{\theta\theta} = \frac{1}{\sqrt{2\pi r}} \cos \frac{\theta}{2} \left(K_I \cos^2 \frac{\theta}{2} - \frac{3}{2} K_{II} \sin \theta \right) \tag{1}$$

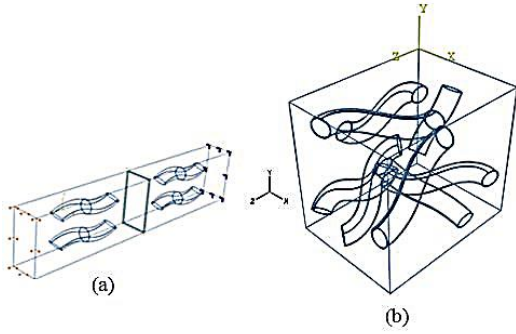


Fig. 3. Distribution of sinusoidal carbon nanotubes (a) uniformly and (b) randomly- distributed.

Where, r and θ are the crack tip coordinates. K_I and K_{II} are the fracture toughness for modes I and II fracture, respectively. These parameters are given by (Ayatollahi et al. 2011):

$$K_I = \frac{M}{Bw^{1/2}} f_I \left(\frac{a}{w} \right) \tag{2}$$

$$K_{II} = \frac{Q}{Bw^{1/2}} f_{II} \left(\frac{a}{w} \right) \tag{3}$$

Where M represents the applied bending moment, B denotes the specimen thickness, W refers to the specimen width, and Q corresponds to the applied shear force. The non-dimensional functions $f_I(a/w)$ and $f_{II}(a/w)$ are defined as the geometric factors for Mode I and Mode II loading, respectively.

According to the Maximum Tangential Stress (MTS) Criterion, fracture initiation occurs in the direction where the tangential stress around the crack tip reaches its peak [13]. To determine the precise angle at which this maximum stress is observed, the tangential stress component $\sigma_{\theta\theta}$ is differentiated with respect to the angle, and the resulting equation is set to zero, as follows:

$$\frac{\partial \sigma_{\theta\theta}}{\partial \theta} = 0 \rightarrow K_I \sin \theta_0 + K_{II} (3 \cos \theta_0 - 1) = 0 \tag{4}$$

The fracture initiation angle θ_0 is obtained using Eq. (4) and serves as a key parameter in predicting the onset of mixed-mode fracture. According to the **Maximum Tangential Stress (MTS) Criterion**, crack propagation occurs when the tangential stress at θ_0 reaches a critical threshold (Ayatollahi

et al., 2011).

Through mathematical derivations, the second assumption of the MTS criterion can be expressed as:

$$K_{IC} = \cos \frac{\theta_0}{2} \left(K_I \cos^2 \frac{\theta_0}{2} - \frac{3}{2} K_{II} \sin \theta_0 \right) \tag{5}$$

Maximum energy release rate criterion

The energy release rate, G , under mixed mode loading is given by [13]:

$$G = \frac{4}{E} \left(\frac{1}{3 + \cos^2 \theta} \right) \left(\frac{1 + \theta/\pi}{1 - \theta/\pi} \right)^{-9/\pi} \times \left[(1 + 3 \cos^2 \theta) K_I^2 + 8 \sin \theta \cos \theta K_I K_{II} + (9 - 5 \cos^2 \theta) K_{II}^2 \right] \tag{6}$$

Where E represents the modulus of elasticity. The **Energy Release Rate Criterion** suggests that crack propagation occurs along an angle θ_0 , where the strain energy release rate attains its maximum value. According to this approach, fracture initiates when the energy release rate at θ_0 reaches a critical threshold, which can be expressed in terms of the critical stress intensity factor K_{IC} . The formulation of the energy release rate criterion is given as [13]:

$$K_{IC} = \left(\frac{2}{3 + \cos^2 \theta_0} \right) \left(\frac{1 + \theta_0/\pi}{1 - \theta_0/\pi} \right)^{-9/2\pi} \left[(1 + 3 \cos^2 \theta_0) K_I^2 + 8 \sin \theta_0 \cos \theta_0 K_I K_{II} + (9 - 5 \cos^2 \theta_0) K_{II}^2 \right]^{0.5} \tag{7}$$

3- Results and Discussion

The simulation outcomes revealed that increasing the CNT content enhances the fracture toughness of nanocomposites. Specifically, the Mode I and Mode II toughness values rose with higher CNT weight fractions in both straight and sinusoidal configurations. However, composites reinforced with straight CNTs consistently outperformed those with sinusoidal CNTs in terms of overall crack resistance. A clear trend was observed: when CNTs are uniformly distributed, the crack paths are more effectively deflected and bridged, resulting in greater energy dissipation and delayed fracture. In contrast, random CNT distributions tend to provide less resistance, particularly in sinusoidal arrangements where orientation misalignment diminishes reinforcement effectiveness. The fracture diagrams generated from simulations closely matched those reported in the literature, validating the modeling strategy. Moreover, the results suggest that the mechanical behavior of CNT-reinforced nanocomposites is strongly dependent not just on the material constituents, but also on the microscopic arrangement and morphology of the reinforcement.

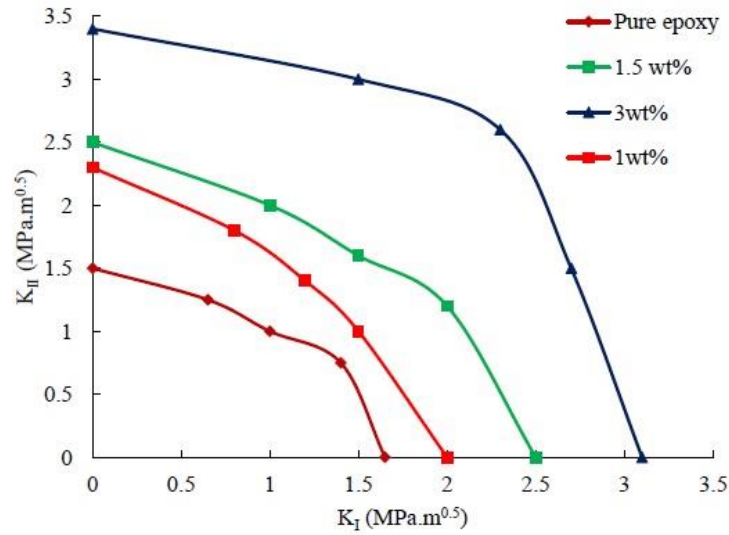


Fig. 4 .KI–KII curves for pure epoxy and nanocomposite reinforced with uniformly distributed straight CNTs.

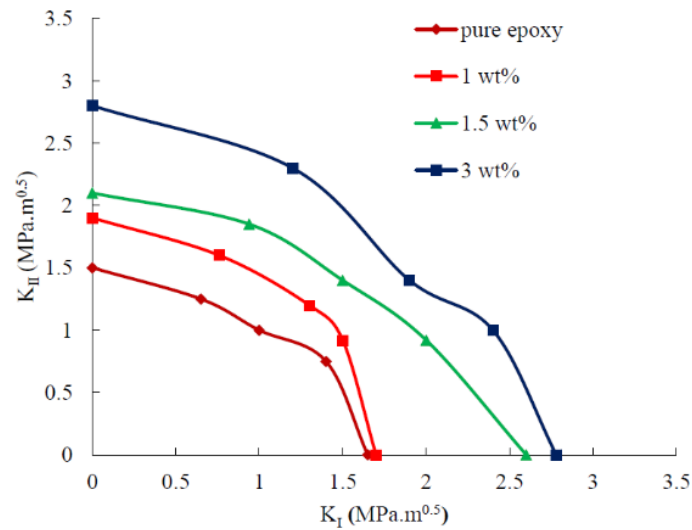


Fig. 5. KI–KII curves for the nanocomposite reinforced with randomly distributed straight CNTs.

This section presents the results for nanocomposites reinforced with straight carbon nanotubes. Initially, an **RVE with a uniform distribution of straight CNTs** was modeled. Various cases were considered, including CNT weight fractions of **1%, 1.5%, and 3%**, to assess their impact on fracture behavior. The findings from these simulations are illustrated in **Figure 4**.

In this figure, mode II fracture toughness is plotted against mode I fracture toughness. As can be observed in this figure, nanocomposite fracture toughness for both modes of fracture increases with CNT weight fraction. The results of this investigation are presented in Fig. 5.

In this figure, Mode II fracture toughness is plotted as a function of Mode I fracture toughness. It is important to note that similar trends observed in Figure 6 also apply to this case. However, the key distinction is that the fracture toughness values for this nanocomposite are lower than those obtained for the uniformly distributed CNT-reinforced composite.

This reduction in fracture toughness can be attributed to the inclined orientation of CNTs relative to the crack propagation path, which affects their ability to effectively bridge and arrest crack growth. The crack propagation paths for both nanocomposite configurations are illustrated in Figures 6 and 7.

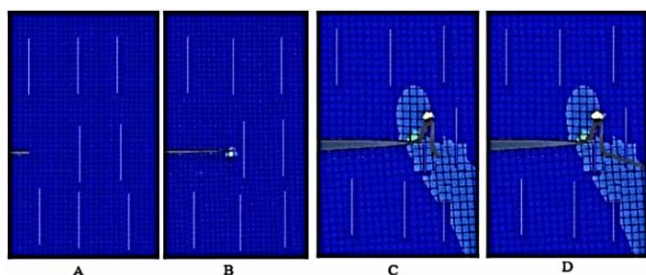


Fig. 6. Crack growth in nanocomposite reinforced with uniformly distributed straight CNTs. (A) to (D) show crack growth path in the nanocomposite.

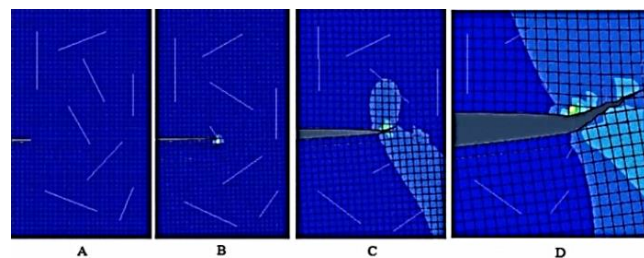


Fig. 7. Crack growth in nanocomposite reinforced with randomly distributed straight CNTs. (A) to (D) show crack growth path in the nanocomposite.

Table 3. Validation of our results with those presented by [13].

Type	Parameter	Current investigation	Ayatollahi et al[13]	Percent Difference
Pure epoxy	K_I	1	0.96	4
	K_{II}	1.82	1.89	3.7
1 wt%	K_I	0	0	0
	K_{II}	2.17	2.2	1.36

Notation: K_I = fracture toughness (mode I); K_{II} = fracture toughness (mode II).

Next, the results of the current investigation are compared with the results presented by [13] to verify our numerical modeling approach. This comparison is presented in Table 3. Note in this table that our results agree well with the reference results.

3- 1- Results of the RVE reinforced with sinusoidal CNTs

This section presents the findings for nanocomposites reinforced with sinusoidal carbon nanotubes. Initially, an RVE with a uniform distribution of sinusoidal CNTs was modeled. Similar to previous cases, CNT weight fractions of 1%, 1.5%, and 3% were considered for analysis. The results obtained from these simulations are illustrated in Figure 8.

In this figure, mode II fracture toughness is plotted against mode I fracture toughness. The results of this investigation are presented in Fig. 9.

In this figure, the mode II fracture toughness is also plotted as a function of the mode I fracture toughness. The key distinction here is that the fracture toughness values of the nanocomposite are lower compared to those observed in a uniformly dispersed CNT nanocomposite. This reduction in toughness is attributed to the inclined orientation of sinusoidal CNTs relative to the crack propagation path, a phenomenon that was similarly noted in the case of straight CNTs.

Following this, the results for the polymer reinforced

with sinusoidal CNTs are analyzed in comparison to those obtained for an RVE containing straight CNT reinforcements. This comparative analysis is illustrated in Table 4 and Fig. 10.

It is important to note that in nanocomposites reinforced with sinusoidal CNTs, the crack propagates along a more linear path compared to those reinforced with straight CNTs. This behavior arises from the fact that, in nanocomposites containing straight CNTs, the crack growth direction tends to be perpendicular to the alignment of the nanotubes.

3- 2- Verification of the Results

To ensure the reliability of the developed numerical model, the simulation results were validated through comparison with both experimental and computational data available in the literature. In particular, the verification process utilized numerical findings reported by Ayatollahi et al. [13] and experimental observations documented by Shadlou et al. [4]. A summary of this comparative evaluation is provided in Table 5.

Note

From the data presented in Table 5, it is evident that the numerical model results align well with those reported in the literature. The differences outlined in the table are based on experimental measurements conducted by Shadlou

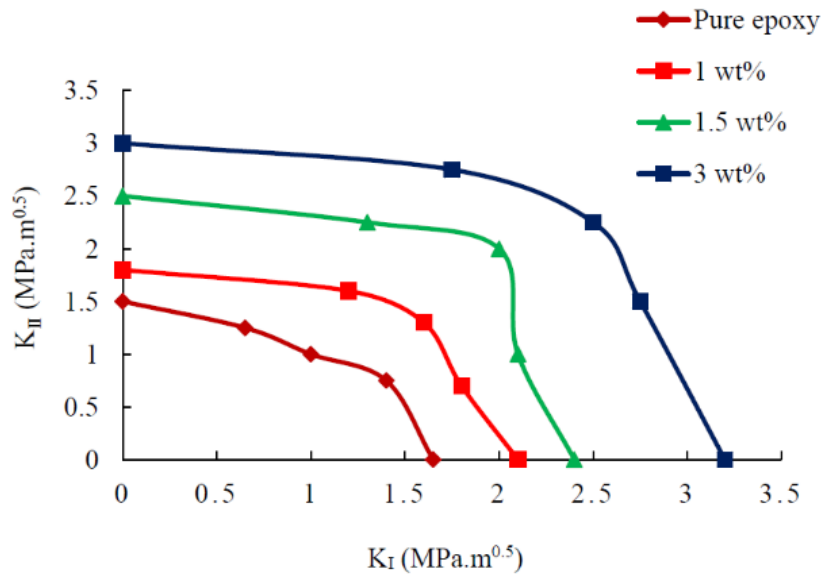


Fig. 8. KI–KII curves for pure epoxy and nanocomposite reinforced with uniformly distributed sinusoidal CNTs.

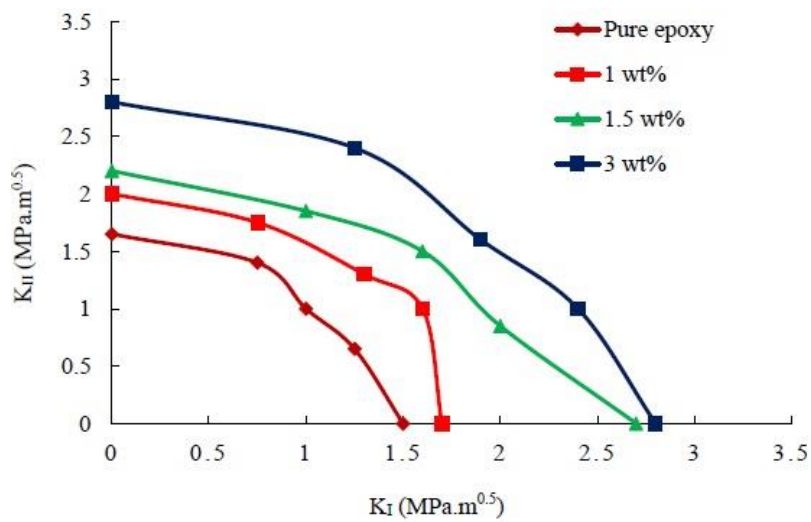


Fig. 9. KI–KII curves for pure epoxy and nanocomposite reinforced with randomly distributed sinusoidal CNTs.

Table 4. Comparison between fracture toughness of nanocomposites reinforced with straight and sinusoidal CNTs. (1.5 wt %).

Case Number	Type and distribution of nanotubes	K_I (MPa.m ^{0.5})	K_{II} (MPa.m ^{0.5})
1	Straight nanotubes (uniformly dispersed)	1	2.3
2	Straight nanotubes (randomly dispersed)	0.94	1.85
-	Percent difference between cases 1 and 2 (%)	6	19.6
3	Sinusoidal nanotubes (uniformly dispersed)	0.5	2
-	Percent difference between cases 1 and 3 (%)	50	13
4	Sinusoidal nanotubes (uniformly dispersed)	0.75	1.6
-	Percent difference between cases 1 and 4 (%)	25	30

Notation: KI= fracture toughness (mode I); KII= fracture toughness (mode II)

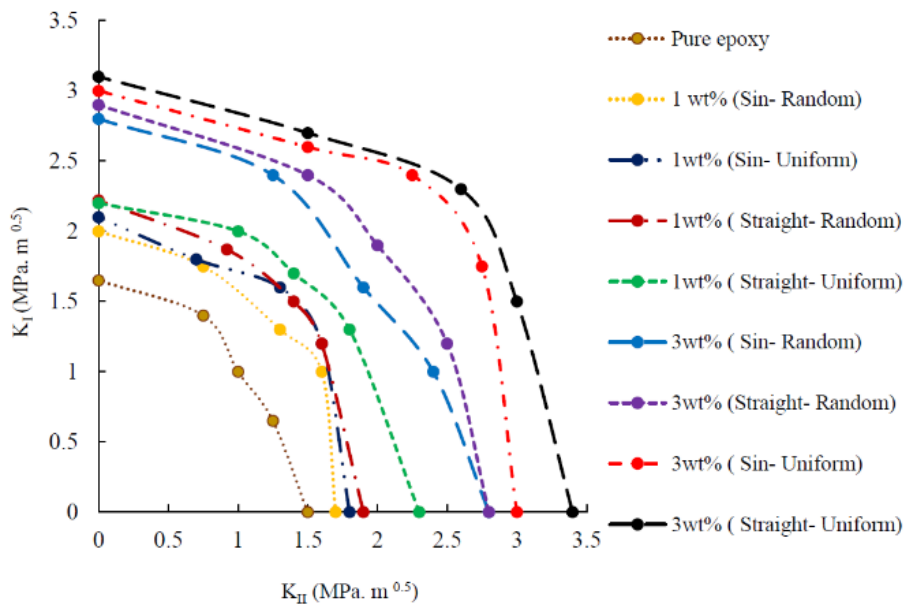


Fig. 10. Comparison of nanocomposites reinforced with straight and sinusoidal carbon nanotubes, randomly and uniformly distribution.

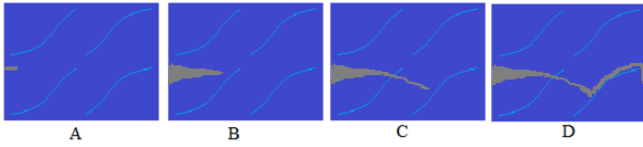


Fig. 11. Crack growth in nanocomposite reinforced with uniformly distributed sinusoidal CNTs. (A) to (D) show crack growth path in the nanocomposite.

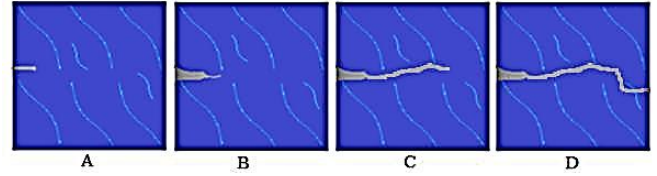


Fig. 12. Crack growth in nanocomposite reinforced with randomly distributed sinusoidal CNTs. (A) to (D) show crack growth path in the nanocomposite.

Table 5. Comparison of the obtained results with literature data [4, 13].

Fracture Toughness Mode	Present Investigation	Ayatollahi et al. [13]	Shadlou et al. [4] Experimental	Difference percent (%) with Experimental Measurements
Mode I (MPa. m ^{0.5})	2.21	2.045±0.1	2.5	11.6
Mode II (MPa. m ^{0.5})	1.61	2.055±0.2	1.5	6.83

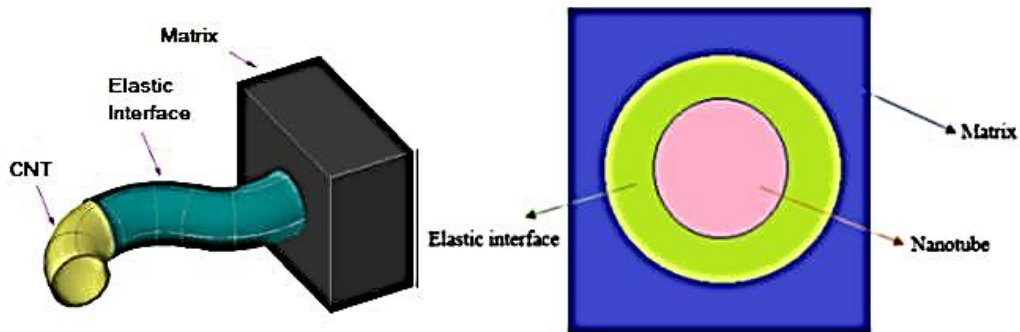


Fig. 13. Schematic of the elastic interface model. A part of each component is shown.

et al. [4], with the largest discrepancy observed in mode I fracture toughness, reaching a maximum of 11.6%. This level of accuracy confirms that the numerical models employed in this study are highly effective in predicting the fracture toughness of nanocomposites.

3- 2- 1- Effects of CNT/matrix interface conditions on the sinusoidal nanotube-reinforced polymer fracture toughness

In this section, the impact of interface conditions on the fracture toughness of sinusoidal CNT-reinforced polymers is analyzed using elastic interface models. To examine the influence of interface strength, a thin elastic layer was incorporated into the model to represent the CNT/matrix

interface. The thickness of this layer was set to 0.14 nm, equivalent to the carbon-carbon bond length [14]. A schematic representation of this model is provided in Fig. 13.

In the case of a perfectly bonded interface between the matrix and the carbon nanotubes, the Mode I fracture toughness is observed to be 1.7. Introducing a compliant (elastic) interfacial layer between the matrix and the CNTs results in a reduction of this value to 1.2. This decline highlights the detrimental effect of the interface layer on load transfer capability, ultimately compromising the material's resistance to crack propagation. Quantitatively, the presence of the interface layer leads to a 29.4% decrease in fracture toughness.

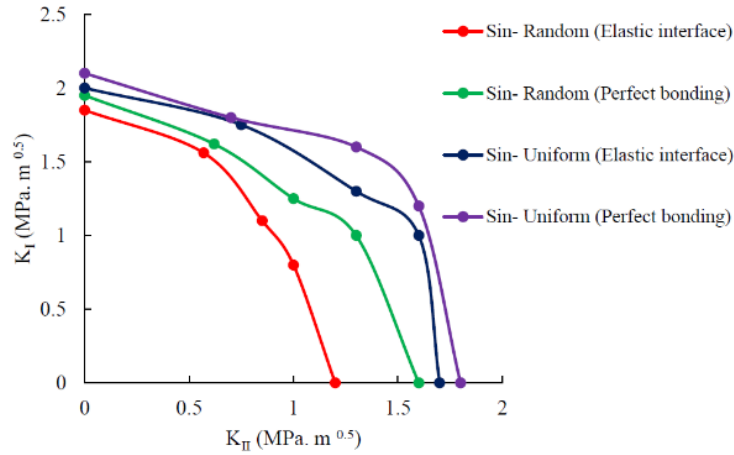


Fig. 14. Comparison between perfect bonding and elastic interface for nanocomposite reinforced with sinusoidal carbon nanotubes.

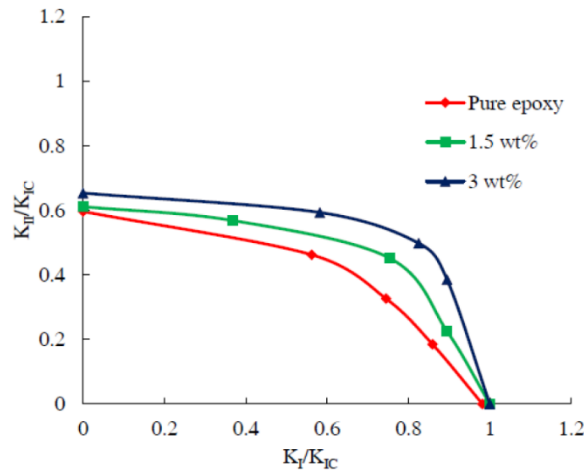


Fig. 15. KI-KIc curves for the nanocomposite reinforced with randomly distributed straight CNTs.

It is important to note that in all cases, the weight fraction of CNTs remains constant at 1%. The corresponding results illustrating this effect are presented in Fig. 14.

3- 2- 2- Maximum Tangential Stress (MTS)

Next, the analysis was performed using the MTS fracture criterion. The results of this investigation are presented in Fig. 15.

Note that the fracture toughness values presented in this figure are presented in non-dimensional form.

3- 2- 3- Maximum energy release rate (G)

This section presents the outcomes derived from applying the energy release rate criterion. The findings corresponding to this analysis are illustrated in Figure 16.

It should be noted that the fracture toughness values presented in this study are dimensionless. As shown in Figure 14, the ratio K_{II}/K_{IC} consistently remains below one, which aligns with the findings reported by Ayatollahi et al. (2011). This observation diverges from the predictions made by the Maximum Tangential Stress (MTS) theory, which does not exhibit this limitation.

To further validate the fracture models, their outputs were systematically compared with numerical data available in the literature, particularly those reported by Ayatollahi et al. [13]. The details of this comparative analysis are summarized in Table 6.

These results pertain to both pure resin and a nanocomposite containing 1.5 wt% of aligned CNTs. It is noteworthy that the obtained results exhibit strong agreement with those

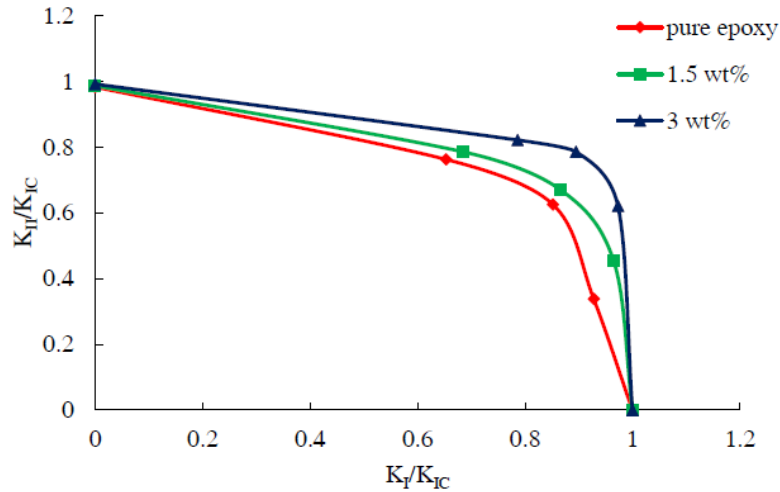


Fig. 16. KI-KIc curves for the nanocomposite reinforced with randomly distributed straight CNTs.

Table 5. Comparison of the obtained results with literature data [4, 13].

Type	Parameter	Current study	Ayatollahi et al. [13]	Percent Difference
Pure epoxy	$K_I/K_{IC}(MTS)$	0	0	0
	$K_{II}/K_{IC}(MTS)$	0.982	0.95	3.25
Pure epoxy	$K_I/K_{IC}(G)$	0	0	0
	$K_{II}/K_{IC}(G)$	0.621	0.61	1.7
1.5 wt% CNT	$K_I/K_{IC}(MTS)$	0	0	0
	$K_{II}/K_{IC}(MTS)$	0.992	0.95	4.2
1.5 wt% CNT	$K_I/K_{IC}(G)$	0	0	0
	$K_{II}/K_{IC}(G)$	0.671	0.635	5.3

Note: K_I = fracture toughness (mode I); K_{II} = fracture toughness (mode II); K_{IC} = critical fracture toughness; MTS= Maximum Tangential Stress; G= Maximum energy release rate

reported in the literature. The largest observed discrepancy, amounting to 5.3%, occurs in the K_{II}/K_{IC} values derived from the energy release rate criterion (G) for the 1.5 wt% CNT-reinforced nanocomposite.

To provide a comprehensive comparison, the results obtained from the two fracture criteria are analyzed across three different cases and illustrated in Figs. 17(a) through 17(c). Specifically, Fig. 17(a) presents the comparative analysis for pure epoxy, offering insights into the fracture

behavior in the absence of CNT reinforcements.

It is important to first note that the energy-release rate criterion (G) systematically predicts lower values of K_{II}/K_{IC} across all values of K_I/K_{IC} . Additionally, K_{II}/K_{IC} shows a slight decrease as K_I/K_{IC} increases, up to approximately 0.6. However, beyond this threshold, the decline in K_{II}/K_{IC} becomes significantly steeper.

Figures 17(b) and 17(c) present results for nanocomposites containing 1.5 wt% and 3 wt% randomly distributed CNTs,

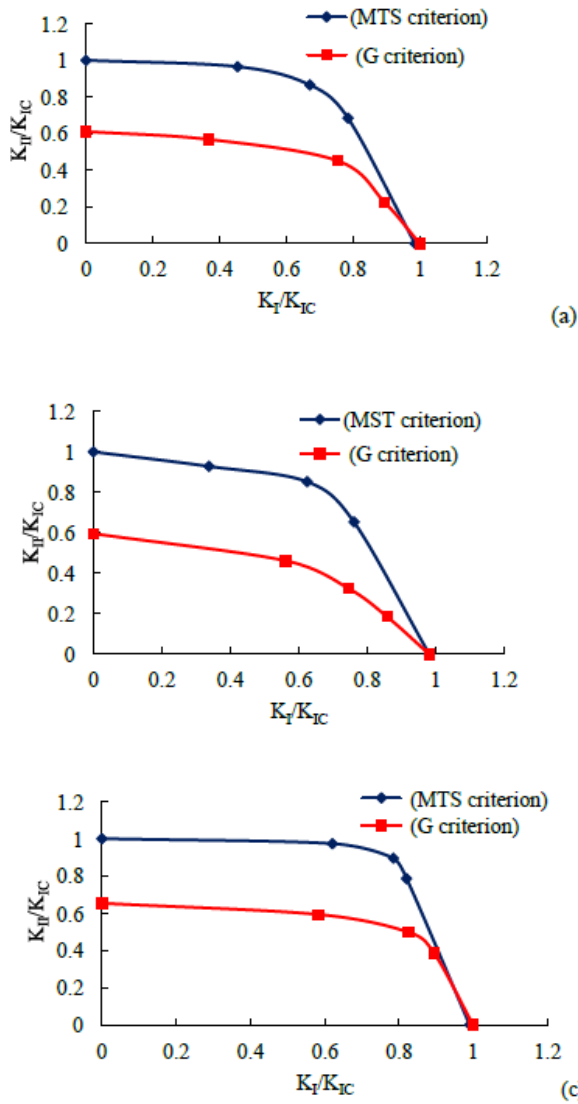


Fig. 17. Comparison of fracture toughness determined using the two criteria: (a) pure epoxy, (b) 1.5 wt. % CNT nanocomposite, (c) 3 wt. % CNT nanocomposite (randomly distributed).

respectively. The findings indicate that K_{II}/K_{Ic} remains nearly constant for $K_I/K_{Ic} \leq 0.6$. Beyond this point, K_{II}/K_{Ic} drops sharply, with the 3 wt% CNT nanocomposite exhibiting an almost vertical drop. This behavior is attributed to the higher CNT content, which alters the fracture response of the nanocomposite.

Furthermore, the energy-release rate criterion (G) suggests that CNT weight fraction has minimal influence on mode II fracture toughness. The overall trends observed for randomly-distributed CNT nanocomposites are consistent with those seen in uniformly distributed CNT nanocomposites. However, a key distinction is that G criterion predicts lower fracture

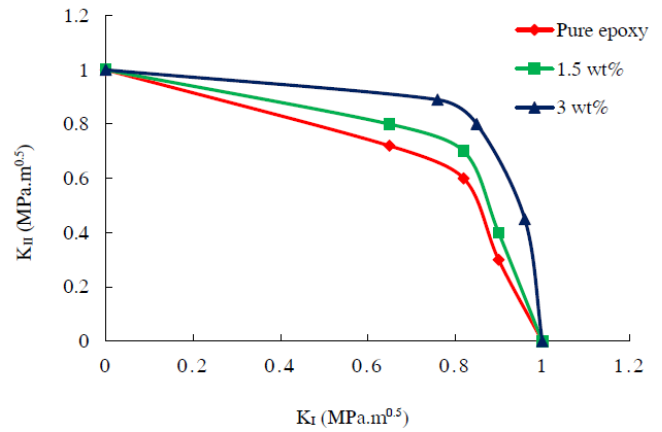


Fig. 18. K_I - K_{Ic} curves for the nanocomposite reinforced with randomly distributed sinusoidal CNTs (MTS).

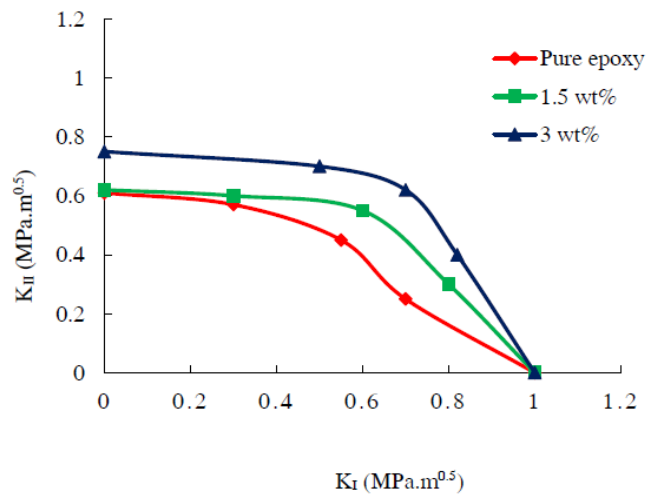


Fig. 19. K_I - K_{Ic} curves for the nanocomposite reinforced with randomly distributed sinusoidal CNTs (G).

toughness values for the randomly distributed CNT case. This discrepancy arises because, in the uniformly distributed CNT nanocomposite, CNTs are predominantly oriented normally to the crack propagation path, thereby enhancing fracture resistance.

3-3- Results of the RVE reinforced with sinusoidal CNTs (MTS and G criteria)

This part of the study focuses on evaluating the fracture toughness behavior of nanocomposites reinforced with randomly distributed sinusoidal carbon nanotubes (CNTs). Both the Maximum Tangential Stress (MTS) and energy

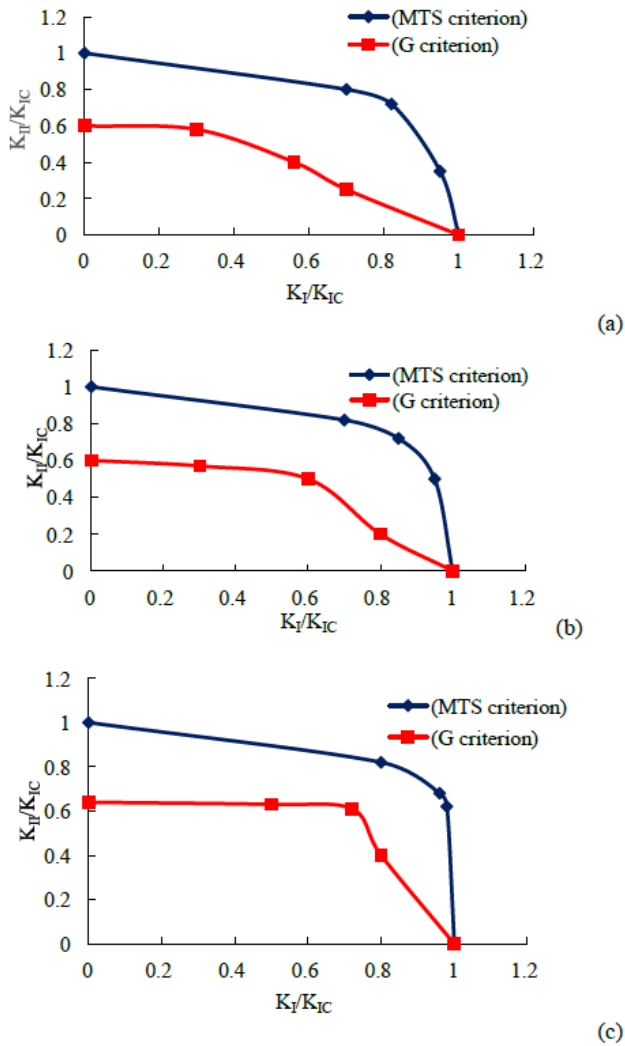


Fig. 20. Comparison of fracture toughness determined using the two criteria: (a) pure epoxy, (b) 1.5 wt. % nanotubes nanocomposite, (c) 3 wt. % CNT nanocomposite (sinusoidal, randomly distributed).

release rate (G) criteria are utilized to determine the critical fracture toughness under Mode I and Mode II loading conditions. This dual approach enables a direct comparison between the theoretical predictions offered by each fracture model. The results of this comparative analysis are illustrated in Figures 18 to 20.

A comparison between Figures 18 and 20 reveals that the Maximum Tangential Stress (MTS) criterion consistently estimates higher fracture toughness values compared to the energy release rate (G) approach. Additionally, as depicted in Figure 20, variations in CNT weight fraction exhibit only a modest influence on the overall fracture toughness of the nanocomposite.

4- Conclusions

This research not only examined the effects of carbon nanotube (CNT) geometry and spatial distribution but also explored how the contact interface between CNTs and the matrix influences the fracture performance of nanocomposites. Mixed-mode fracture simulations were performed using the finite element software ABAQUS. The main conclusions derived from the study are outlined below:

1. Impact of CNT Content: An increase in CNT weight fraction enhances the fracture toughness of the nanocomposite, underscoring the reinforcing role of CNTs in crack resistance.

2. Role of CNT Geometry: Composites reinforced with straight CNTs showed superior fracture toughness compared to those containing sinusoidal CNTs, emphasizing the critical role of nanotube morphology in mechanical performance.

3. Crack Growth Behavior: Crack propagation occurred more rapidly in composites reinforced with sinusoidal CNTs, indicating that these configurations provide lower resistance to fracture.

4. Fracture Initiation Threshold: In all cases, crack initiation was triggered once the fracture toughness approached the material's critical value, confirming a distinct onset point for failure.

5. Evaluation of Fracture Models: The Maximum Tangential Stress (MTS) criterion consistently predicted higher toughness values compared to the energy release rate method (G), suggesting that MTS offers a more conservative assessment of fracture resistance.

6. Effect of Interfacial Layer: The inclusion of a compliant interface between CNTs and the matrix resulted in reduced fracture toughness, attributed to diminished load transfer capabilities.

These findings offer critical insights into the design and optimization of CNT-reinforced nanocomposites, highlighting the importance of nanotube shape, dispersion, and interfacial bonding in determining their fracture behavior.

References

- [1] F. H. Gojny, M. H. G. Wichmann, U. Kopke, B. Fiedlerand, K. Schulte, Carbon nanotube-reinforced epoxy-composites: enhanced stiffness and fracture toughness at low nanotube content, *Composites Science and Technology*, 64 (2004) 2363–2371.
- [2] M. Quaresimin, M. Salviato, M. Zappalorto, A multi-scale and multi-mechanism approach for the fracture toughness assessment of polymer nanocomposites, *Composites Science and Technology*, 91 (2014) 16–21.
- [3] M. H. Meliani, Z. Azari, M. Al-Qadhi, N. Merah, G. Pluvinae, A two-parameter approach to assessing notch fracture behavior in clay/epoxy nanocomposites, *Composites Part B*, 80 (2015) 126–130.
- [4] S. Shadlou, E. Alishahi, M. R. Ayatollahi, Fracture behavior of epoxy nanocomposites reinforced with different carbon nanoreinforcements, *Composite Structures*, 95 (2013) 577–581.
- [5] M. Golestanian, M. Hamed, Fracture Analysis of Sinusoidal CNT-Based Nanocomposites with Uniform

- and Nonuniform CNT Distributions, *International Journal of Structural Stability and Dynamics*, 10(4) (2015) 1550058.
- [6] M. Hosseini, K. Majidi Mozafari, Stability Analysis of a Functionally Graded Carbon Nanotube Reinforced Composite Plate Integrated with Piezoelectric Layers under Supersonic Airflow, *AUT Journal of Mechanical Engineering*, 6(4) (2022) 525–544.
- [7] S. Dastjerdi, Ö. Civalek, M. Malikan, B. Akgöz, On analysis of nanocomposite conical structures, *International Journal of Engineering Science*, 191 (2023) 103918.
- [8] S. , G. Arani, Z. Khoddami Maraghi, Arshid, Free vibration and supersonic flutter analyses of a sandwich cylindrical shell with CNT-reinforced honeycomb core integrated with piezoelectric layers, *Mechanics Based Design of Structures and Machines*, (2024).
- [9] Z. Khoddami Maraghi, [Title missing], *Journal of Sound and Vibration*, 457 (2019) 240–260.
- [10] H. Akbas, , Numanoglu, , Ö. Civalek, Application of Newmark Average Acceleration and Ritz Methods on Dynamical Analysis of Composite Beams under a Moving Load, *Journal of Applied and Computational Mechanics*, 8(2) (2023) 764–773.
- [11] M. Hamed, H. Golestanian, Y. Tadi Beni, K. Alasvand Zarasvand, Evaluation of fracture energy for nanocomposites reinforced with carbon nanotubes using numerical and micromechanical methods, *Mechanics of Materials and Structures*, 0(0) (2018) 1–9.
- [12] X. L. Chen, Y. J. Liu, Square representative volume elements for evaluating the effective material properties of carbon nanotube-based composites, *Computational Materials Science*, 29 (2004) 1–11.
- [13] M. R. Ayatollahi, S. Shadlou, M. M. Shokrieh, Mixed mode brittle fracture in epoxy/multi-walled carbon nanotube nanocomposites, *Engineering Fracture Mechanics*, 78 (2011) 2620–2632.
- [14] H. Golestanian, M. Shojaie, Numerical characterization of CNT-based polymer composites considering interface effects, *Computational Materials Science*, 50 (2010) 731–734.

HOW TO CITE THIS ARTICLE

M. Hamed, *Comparison of Fracture Behavior Between Nanocomposites Reinforced with Straight and Sinusoidal Carbon Nanotubes*, *AUT J. Mech Eng.*, 9(3) (2025) 249-264.

DOI: [10.22060/ajme.2025.23665.6150](https://doi.org/10.22060/ajme.2025.23665.6150)



